Applied Catalysis B: Environmental 242 (2019) 9–18

Contents lists available at ScienceDirect

Applied Catalysis B: Environmental

journal homepage: www.elsevier.com/locate/apcatb

The roles of pyrite for enhancing reductive removal of nitrobenzene by zero-valent iron

Ying Lü[a], Jianfa Li[a], Yimin Li[a,*], Liping Liang[b], Huaping Dong[a], Kun Chen[a], Chunxia Yao[a], Zhanfeng Li[a], Jinxiang Li[c], Xiaohong Guan[c,d,**]

[a] College of Chemistry and Chemical Engineering, Shaoxing University, Huancheng West Road 508, Shaoxing, Zhejiang, 312000, PR China
[b] College of Life Sciences, Shaoxing University, No. 900, South City Road, Shaoxing, Zhejiang, 312000, PR China
[c] State Key Laboratory of Pollution Control and Resource Reuse, College of Environmental Science and Engineering, Tongji University, Shanghai, 200092, PR China
[d] Shanghai Institute of Pollution Control and Ecological Security, Shanghai, 200092, PR China

ARTICLE INFO

Keywords:
Pyrite
Zero valent iron
Reduction
Nitrobenzene
Synergetic effect

ABSTRACT

Zero-valent iron (ZVI) is a popular reductant that has been successfully applied for remediation of groundwater contaminated with various pollutants, but it still suffers from surface passivation and pH increase in the reaction media. In this study, pyrite, a ubiquitous sulfide mineral in anaerobic environment, was adopted to enhance the reactivity of ZVI for removal of nitrobenzene. The synergetic effect between pyrite and ZVI was observed for nitrobenzene reduction, and the rate constant k_{obs} at the initial pH (pH_0) 6.0 was enhanced by 8.55–23.1 folds due to the presence of pyrite with pyrite/ZVI mass ratio ranging from 1.0 to 6.0. Moreover, nitrobenzene could be removed effectively at pH_0 ranging from 5.0 to 10.0 in the presence of pyrite, while negligible removal of nitrobenzene by ZVI (0.5 g/L) alone was observed at $pH_0 \geq 7.0$. ZVI sample recovered from the reacted ZVI/pyrite mixture was also more effective for nitrobenzene degradation than pristine ZVI. The mechanism study revealed that pyrite could suppress the pH increase in reaction media, boost the production of reactive Fe^{2+}, and activate the ZVI surface through replacing partially the passive oxide film with iron sulfide (FeS). In particular, the formation of highly reactive FeS@Fe in the reaction system of ZVI/pyrite mixture was proved by XRD, Mössbauer, XANES, XPS and SEM-EDS analyses, which provides a facile way for *in-situ* sulfidation of ZVI and for enhancing the removal of contaminants with ZVI technology.

1. Introduction

Zero-valent iron (ZVI) is a readily available, inexpensive, nontoxic and moderately strong reducing agent, and thus various organic and inorganic compounds have been successfully removed from the aqueous phase by using ZVI [1–7]. Since the 1990s, *in-situ* remediation technologies such as permeable reactive barrier (PRB) using ZVI as the reactive material have been successfully applied for remediation of groundwater contaminated with various pollutants [8,9]. However, due to the direct involvement of H^+ in the reactions of ZVI with contaminants and water, pH of the reaction mixture often increases with reaction time. Moreover, the precipitation of iron (hydr)oxides on ZVI surface may passivate ZVI, which is more severe at higher pH and can result in a drop in the reactivity of ZVI [10]. Over the last decades, many methods such as fabrication of nanoscale ZVI [11–15], using bimetal materials [16–18], employing physical measures such as weak magnetic field [5,19], coating with carboxymethyl cellulose [20] or aluminum hydroxide [21], and dispersing ZVI nanoparticles on supports such as clays [22,23], carbons [24,25] and polymers [26,27] have been developed to enhance the reactivity of ZVI and expand its working pH range. Recently, one modification to ZVI technology that has shown great promise for improving the efficiency of contaminant treatment is sulfidation, which is defined, for ZVI-based systems, as the result of any treatment that forms iron sulfides (FeS_x) secondary phases in place of, on the surface of, or in close association with the primary ZVI and iron oxide phases [28–30]. Up to now, most of the published researches about sulfidation focused on the nanoscale ZVI, and the reported sulfidation methods employed sulfur compounds of various oxidation states, including elemental sulfur, Na_2S, $Na_2S_2O_4$, and $Na_2S_2O_3$, to treat ZVI *via* either one-step method or two-step method [31–34]. In

* Corresponding author.
** Corresponding author at: State Key Laboratory of Pollution Control and Resource Reuse, College of Environmental Science and Engineering, Tongji University, Shanghai 200092, PR China.
E-mail addresses: liym@usx.edu.cn (Y. Li), guanxh@tongji.edu.cnd (X. Guan).

https://doi.org/10.1016/j.apcatb.2018.09.086
Received 7 June 2018; Received in revised form 21 September 2018; Accepted 27 September 2018
Available online 30 September 2018
0926-3373/

comparison with nanoscale ZVI, the microscale ZVI is cheaper and more economical for practical applications, so sulfidation was also extended to the microscale ZVI recently [35,36], and a ball milling method has been developed for the easier and safer operation [31,37].

Pyrite (FeS_2) is the most common species of iron sulfide minerals that are widely distributed in anaerobic environment as the major product of sulfate reduction by bacteria [38] and is also found in the reactive materials of commercially installed ZVI-PRB [8]. Since both Fe (II) and disulfide species in pyrite can serve as electron donors, many efforts have been made to develop efficient approaches with pyrite as reductant for removing a variety of pollutants such as chlorinated organic compounds (COCs), chromate, selenate and selenite [38–44]. Generally, pyrite is less reactive than ZVI, because pyrite possesses a more positive standard reduction potential (+0.35 V) than ZVI (−0.44 V) and different reduction mechanisms from ZVI [45–47]. However, the oxidation of pyrite releases H^+ (Eqs. (2) and (3)) [45], which can result in a significant drop in pH in the reaction media to an acid level [48]. Compared to O_2, Fe^{3+} can oxidize pyrite abiotically and anaerobically *via* Reaction (2) more rapidly [49]. Since pyrite is a ubiquitous mineral in reducing environments [50], it may influence the performance of groundwater remediation by ZVI. Because pyrite will react with Fe^{3+} generated during contaminants removal by ZVI, and regeneration of both Fe^{2+} and H^+ *via* Reaction (2) will in turn accelerate the reductive removal of contaminants by ZVI. Although there have been a few reports that pyrite could enhance the degradation rate of trichloroethylene and carbon tetrachloride by ZVI [51,52], the inherent mechanisms for such enhancement remains unclear. In particular, the specific roles of pyrite on influencing the pH change, Fe^{2+} cycling and ZVI surface passivation during the removal of contaminants have never been addressed.

$$2Fe^0 + O_2 + 2H_2O \rightarrow 2Fe^{2+} + 4OH^- \quad (1)$$

$$FeS_2 + 14Fe^{3+} + 8H_2O \rightarrow 15Fe^{2+} + 2SO_4^{2-} + 16H^+ \quad (2)$$

$$FeS_2 + {}^{7}\!/_{2}O_{2(aq)} + H_2O \rightarrow Fe^{2+} + 2SO_4^{2-} + 2H^+ \quad (3)$$

Nitrobenzene occurs as a pollutant in groundwater mainly originating from various industrial processes such as the manufacture of aniline, pharmaceuticals, dyes, pesticides as well as its wide application and improper disposal [53]. Nitrobenzene is relatively toxic and persistent in the environment, and is listed as a priority pollutant by many countries [54]. Thus, the specific objectives of this study are: 1) to investigate the influence of pyrite on nitrobenzene reduction by ZVI as functions of pyrite dosage and initial pH; 2) to explore the roles of pyrite on enhancing nitrobenzene removal by ZVI.

2. Experimental

2.1. Chemical and reagents

The pyrite ore purchased in Yingde, Guangdong Province of China was used for preparing pyrite sample with a size between 200–300 meshes through a purification procedure [46,55], and the details are described in Text S1 of the Supporting Information (SI). X-ray fluorescence (XRF) analysis (XRF-1800, Shimadzu, Japan) of the pyrite sample indicated that it contained 46.0% Fe and 52.2% S (mass content), equivalent to a purity of 98.2%. X-ray diffraction (XRD) pattern of the pyrite sample is in agreement with that of the standard sample (JCPDS 06-0710). ZVI was purchased from Aladdin Reagents (Shanghai) Co. Ltd., and the powder with a size similar to that of pyrite was pretreated with the same procedure as pyrite, and Fe content of the clean ZVI sample was determined to be 97.7% (by mass). BET specific surface areas of pyrite and ZVI samples, measured with N_2 adsorption isotherms at 77 K (Autosorb IQ, Quantachrome Instruments, USA), were 0.183 and 0.415 m^2/g, respectively. Nitrobenzene (AR), Aniline (> 99.0%, ACS), Nitrosobenzene (> 98%, GC grade), N-Phenylhydroxylamine (> 98%, HPLC grade), 1,10-Phenanthroline monohydrate (98%, AR), Methanol (> 99.9%, HPLC grade), Tween™ 80 (Medicinal grade), ethanol absolute (99.5%, Medicinal grade), concentrated HCl (37%, AR) were purchased from Aladdin Reagents (China). Barium chloride dehydrate (AR) was obtained from Sinopharm Chemical Reagent Co., Ltd. The solution of nitrobenzene was prepared with 18.2 MΩ cm (Milli-Q Gradient, Millipore, USA) pure water that was de-oxygenated with pure N_2 for 1 h under ambient conditions.

2.2. Batch removal experiments

The removal experiments of nitrobenzene were carried out in triplicates under anaerobic conditions, and the loading operation was conducted in a glove box purged with N_2. To determine the influence of pyrite dosage on nitrobenzene decomposition, 150 mL of nitrobenzene solution with initial concentration (C_0) of 0.2031 mmol/L (25.0 mg/L) was added into a glass bottle with volume of 250 mL, and the initial pH (pH_0) of solution was adjusted to 6.0 with 0.01 M HCl. The reaction was initiated by adding 0.5 g/L of ZVI and 0.5–3.0 g/L of pyrite into the bottle, which was immediately sealed with a stopper and aluminum foil. To investigate the removal of nitrobenzene at various pH_0, pH_0 of nitrobenzene solution was adjusted to 5.0–10.0 with 0.01 M HCl and/or 0.01 M NaOH, followed by dosing ZVI (0.5 g/L) and pyrite (2.0 g/L). Then, the loaded bottle was moved out of the glove box, placed in a dark thermostatic shaker bath at 25 ± 0.2 °C, and shaked at a rotating speed of 200 rpm. The kinetics of nitrobenzene degradation with ZVI alone or pyrite alone was also determined with the same procedure to work as control. At fixed periods, approximately 1 mL of the suspension was withdrawn and filtered with a 0.22 μm membrane filter. The obtained filtrate was kept for further analysis. The nitrobenzene (NB) disappearance kinetics was simulated with the pseudo-first-order Reaction model (Eq. (4)).

$$\frac{d[\mathrm{NB}]}{dt} = -k_{\mathrm{obs}}[\mathrm{NB}] \quad (4)$$

2.3. Analysis of solution samples

The concentrations of nitrobenzene and its reduction products were determined with a LC-20AT HPLC system (Shimadzu, Japan) equipped with an ultraviolet detector (the wavelength was set at 270 nm). The column used was an Agilent Extend-C18 analytical column (4.6 mm × 250 mm, 5 μm), and the mobile phase was the mixture of methanol and pure water (V/V = 65/35). Solution pH was monitored with a pH meter (FE28, Mettler Toldo, Switzerland), and the concentration of Fe^{2+} was measured with the phenanthroline photometric method (UV-2800, UNICO, China). The two phases (solid and liquid) of the reaction system were separated by decantation for determining SO_4^{2-} generated in the reaction. The concentration of SO_4^{2-} in supernatant was determined with ionic chromatography (HIC-SP, Shimadzu, Japan), and SO_4^{2-} in the solid residual was determined with barium sulfate turbidimetry after acid dissolution [56]. For this purpose, the solid residual was soaked in 25 mL of 0.1 M HCl twice, and then rinsed with de-oxygenated pure water. The total solutions collected in soaking and rinsing were transferred into a 100 mL volumetric flask and diluted to 100 mL with de-oxygenated pure water. The SO_4^{2-} concentration in the clear liquid after filtration with 0.22 μm membrane was calculated from the absorbance of barium salt at 420 nm (UV-2800, UNICO, China). Turbidimetry was used here instead of ionic chromatography to avoid the disturbance of Cl- rich in the soaking solution.

2.4. Characterization of solid samples

The solid residues after reaction in the combined ZVI/pyrite system were collected by filtration with N_2 protection, and freeze-dried in vacuum. The residual ZVI sample was magnetically separated from the

collected dry solids and used for spectroscopic analysis. The crystalline substances contained in the recycled ZVI sample were analyzed by XRD using X'Pert PRO (PANalytical B.V., Netherlands) equipment with CuKα radiation. Mössbauer spectrum of the recycled ZVI sample was collected at 78 K using a Topologic 500 A spectrometer and a proportional counter. A ^{57}Co(Rh), moving with a constant acceleration mode, was used as the γ-ray radioactive source. The velocity was calibrated by a standard α-iron foil. The Mössbauer spectra were fitted using the MossWinn software. The surface compositions of the recycled ZVI samples were investigated with X-ray photoelectron spectroscopy (XPS) using a Thermo ESCALAB 250 system (USA) with a monochromatized Al Kα X-ray source ($h\nu$ = 1486.6 eV) operated at a power of 150 W. The binding energies of photoelectrons were corrected by C 1s peak at 284.8 eV. Changes in surface mineral phase of active materials before and after reaction were characterized with a scanning electron microscope (SEM) (JEOL JSM-6360LV) equipped with an X-act energy dispersive X-ray spectrometer (EDS) (Oxford). Synchrotron-radiation based bulk X-ray adsorption spectroscopy (XAS) was used to examine S speciation in the ZVI sample recycled from the combined ZVI/pyrite system. X-ray absorption near-edge structure (XANES) spectroscopy was carried out at Beijing Synchrotron Radiation Facility (BSRF) located at Institute of High Energy Physics, Chinese Academy of Science in Beijing, China. Sulfur K-edge XANES data were recorded in total electron yield (TEY) model at ambient temperature and scanned at step width of 1.0 eV in the region between 2.45 KeV and 2.52 KeV. Na_2SO_4, Na_2SO_3, S, FeS_2 and FeS were analyzed as reference standards. Spectral data were normalized to the maximum of the absorption spectrum using Athena XAS data analysis software.

3. Results and discussion

3.1. Enhancing effect of pyrite on reductive removal of nitrobenzene by ZVI

The kinetics of nitrobenzene removal by ZVI, pyrite, and the mixture of ZVI and pyrite at pH_0 6.0 are demonstrated in Fig. 1. ZVI (0.5 g/L) or pyrite (2.0 g/L) alone is not effective for nitrobenzene removal, as shown in Fig. 1(a) and (b), and only ~0.03 mM nitrobenzene is removed by either ZVI or pyrite in 300 min. There were negligible reduction products of nitrobenzene observed in the process of nitrobenzene removal by pyrite, indicating that nitrobenzene was removed by pyrite *via* adsorption rather than reduction. This is because it is difficult for the release of Fe^{2+} and S_2^{2-} (the two species with reductive reactivity) from pyrite at the pH (~6.0) used in this experiment. Zhang et al. [48] observed the reduction of nitrobenzene by pyrite, which may be ascribed to the very high dosage of pyrite (30 g/L) employed in their study. However, nitrobenzene could be reduced by ZVI to aniline with nitrosobenzene and N-phenylhydroxyamine as the intermediates, similar to that reported previously with ZVI dosage ranged from 13.3 to 33.3 g/L [57–59], although the reaction rate is slower in this study due to the much smaller dosage (only 0.5 g/L). The removal of nitrobenzene by ZVI was dramatically accelerated with the addition of pyrite, and a higher dosage of pyrite had a larger augmenting effect, as illustrated in Fig. 1(c) and (d). The liquid chromatograms of aqueous samples collected from the reaction system of nitrobenzene reduction by ZVI/pyrite mixture after different reaction time (30, 60, 120 and 180 min), under the reaction conditions identical to those of Fig. 1(d), are depicted in SI Fig. S1. The disappearance of nitrobenzene was accompanied with the appearance of nitrosobenzene, phenylhydroxylamine, and aniline while both nitrosobenzene and phenylhydroxylamine were further transformed to aniline. The increase in pyrite dosage promoted the transformation of nitrobenzene to aniline, indicating that pyrite appreciably facilitated the reductive removal of nitrobenzene by ZVI.

The influence of pyrite on nitrobenzene removal by ZVI at various pyrite dosages was further investigated, as illustrated in Fig. 2. At the same pH_0 6.0, the removal rate of nitrobenzene increased gradually with the pyrite dosage increasing from 0.5 to 2.0 g/L, while further increase of pyrite dosage to 3.0 g/L did not show more significant improvement on the removal rate. At the same dosage of ZVI and pyrite, the influence of pH_0 on nitrobenzene removal was explored as well. The improving effect of pyrite was more remarkable at higher pH_0, as illustrated in SI Fig. S2. Without pyrite, the removal of nitrobenzene by ZVI was negligible at $pH_0 \geq 7.0$, consistent with results reported in the literature [58,59]. However, nitrobenzene could be removed effectively at pH_0 ranging from 5.0 to 10.0 in the presence of pyrite, suggesting that the presence of pyrite remarkably expanded the working pH range of ZVI for nitrobenzene reduction.

To quantify the accelerating effect of pyrite on nitrobenzene removal by ZVI, the kinetics of nitrobenzene sequestration by ZVI with the presence of pyrite at the beginning of the reaction (0–60 min) under different conditions was simulated with the *pseudo*-first-order rate law. The obtained rate constants (k_{obs}) are summarized in Fig. 3. With the increase of mass ratio of pyrite/ZVI from 0 to 4.0 at pH_0 6.0, the k_{obs} increased progressively from 1.1×10^{-3} to 24.6×10^{-3} min^{-1} and it leveled off with a further increase in the mass ratio of pyrite/ZVI to 6.0. The rate constant of nitrobenzene reduction by ZVI at pH_0 6.0 was enhanced by 8.55–23.1 folds because of the presence of pyrite with pyrite/ZVI mass ratio ranging from 1.0 to 6.0 (Fig. 3(a)). When the pyrite/ZVI mass ratio was fixed at 4.0, the k_{obs} of nitrobenzene removal by pyrite/ZVI mixture descended progressively from 23.1×10^{-3} min^{-1} to 4.4×10^{-3} min^{-1} with increasing pH_0 from 6.0 to 10.0, while it elevated slightly from 21.8×10^{-3} min^{-1} to 23.1×10^{-3} min^{-1} as pH_0 increased from 5.0 to 6.0, as shown in Fig. 3(b). Over the pH range investigated in this study, nitrobenzene removal by ZVI/pyrite mixture was much higher than the sum of nitrobenzene removed separately by ZVI and pyrite, indicating the synergetic effect between pyrite and ZVI for removal of nitrobenzene.

The enhancing effect of pyrite on the reactivity of ZVI for nitrobenzene removal is supported by another interesting fact that the ZVI sample recycled from the combined ZVI/pyrite system still maintained high reactivity. Fig. 4 shows the kinetics of nitrobenzene removal for five repetitive runs by ZVI/pyrite mixture and ZVI alone as well as four repetitive runs using the iron sample (ZVI^{pyr}) separated from the ZVI/pyrite mixture after reaction in the first run. The ZVI/pyrite mixture could completely remove the applied nitrobenzene within 300 min in the first four repetitive runs and over 94% of the dosed nitrobenzene could be removed even in the fifth run. Although only 8.2%–17.5% of the dosed nitrobenzene could be removed by pristine ZVI in each run, ZVI sample recovered from the reacted ZVI/pyrite mixture was much more effective and could remove 54.8%–70.4% of nitrobenzene in each run. The above results indicated that pyrite could activate ZVI, making ZVI much more reactive than the pristine sample. So, application of the ZVI/pyrite mixture in PRB should be a good idea for removing pollutants, although the efficiency in the real groundwater remediation process needs to be validated before such application. And according to the above results, the ZVI-PRB installed in the pyrite-rich area should show higher removal efficiency than the ZVI-PRB installed in the area without pyrite.

3.2. Effect of pyrite on suppressing the pH increase in reaction system

Fig. 5 shows the change of pH with time during the reaction of nitrobenzene with ZVI, pyrite, and pyrite/ZVI mixture at pH_0 6.0. pH of the pyrite system varied slightly from 6.0 to 6.3, which was consistent with the negligible nitrobenzene reduction by pyrite alone. As expected, pH in the reaction media of nitrobenzene and ZVI increased sharply from 6.0 to 8.1 in 10 min and then stabilized at 8.5-8.7. The application of pyrite could keep pH of the ZVI/pyrite system much lower than that in the system of ZVI alone (8.5–8.7), and higher dosage of pyrite resulted in lower pH. The inhibiting effect of pyrite on pH elevation should be mainly ascribed to the oxidation of pyrite by Fe^{3+} (Eq. (2)), which is an effective pyrite oxidant at both acid and neutral

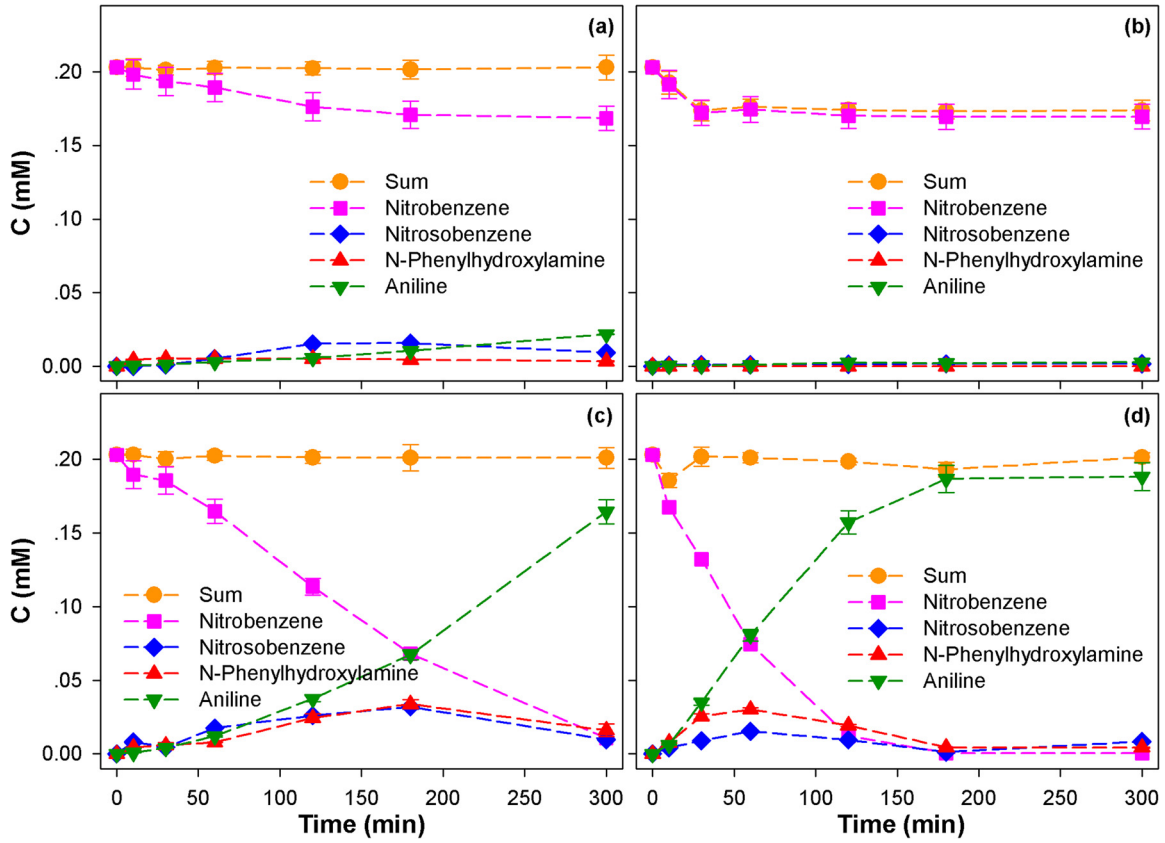

Fig. 1. Concentration changes of nitrobenzene, aniline, and intermediates (nitrosobenzene and N-phenylhydroxyamine) as well as the mass balance in aqueous phase during nitrobenzene removal by (a) 0.5 g/L ZVI, (b) 2.0 g/L pyrite, (c) 0.5 g/L ZVI + 0.5 g/L pyrite, and (d) 0.5 g/L ZVI + 2.0 g/L pyrite at pH_0 = 6.0.

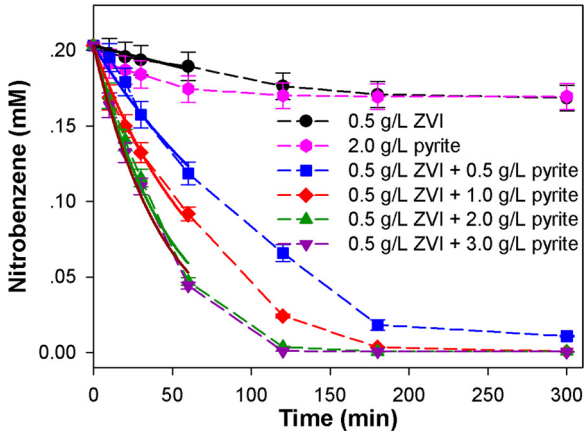

Fig. 2. Nitrobenzene removal by ZVI, pyrite, and their mixture with different pyrite dosages at pH_0 = 6.0.

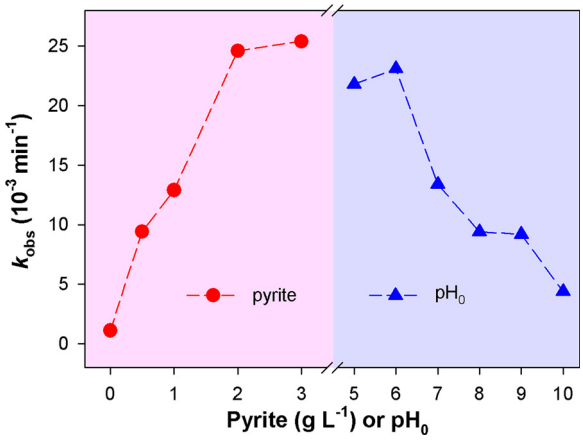

Fig. 3. Influence of pyrite dosage (a) and pH_0 (b) on the pseudo-first-order rate constants (k_{obs}) of nitrobenzene reduction by ZVI/pyrite mixture. Reaction conditions: (a) pH_0 = 6.0, ZVI = 0.5 g/L; (b) ZVI = 0.5 g/L, pyrite = 2.0 g/L.

pH [45,60]. Fe^{3+} may derive from further oxidation of Fe^{2+} generated from the reaction of Fe^0 with nitrobenzene (Eq. (5)), and more details about the transformation of iron species (Fe^0, Fe^{2+}, and Fe^{3+}) will be discussed in the following section. According to the literature, lower pH could facilitate the corrosion of ZVI and thus accelerate nitrobenzene reduction [59]. As illustrated in SI Fig. S3, pH of the combined ZVI/pyrite system was always stabilized at the value lower than that of ZVI system, regardless of the pH_0. Thus, benefiting from pyrite on suppressing the pH increase in reaction media, the ZVI/pyrite mixture exhibited good adaptability to pH variation.

$$3Fe^0 + Ar{-}NO_2 + 6H^+ \rightarrow 3Fe^{2+} + Ar{-}NH_2 + 2H_2O \quad (5)$$

To identify the contribution of pyrite (2.0 g/L) due to suppressing pH increase, pH of the system of removing nitrobenzene by ZVI at pH_0 6.0 was manually controlled at ~6.8 with dilute HCl solution and the kinetics of nitrobenzene by ZVI under this reaction condition was shown in SI Fig. S4. The reaction was indeed accelerated by pH regulation, with the k_{obs} enhanced to $3.90 \times 10^{-3}\,min^{-1}$, a value equivalent to only ~15.9% of that obtained in the combined ZVI/pyrite system ($2.46 \times 10^{-2}\,min^{-1}$). Moreover, the removal of nitrobenzene by the combined ZVI/pyrite system at pH_0 10.0 was much faster than that by ZVI alone at pH_0 5.0–6.0. Consequently, there must be other functions of pyrite, besides suppressing pH increase, contributing to the enhanced removal of nitrobenzene in the combined ZVI/pyrite system.

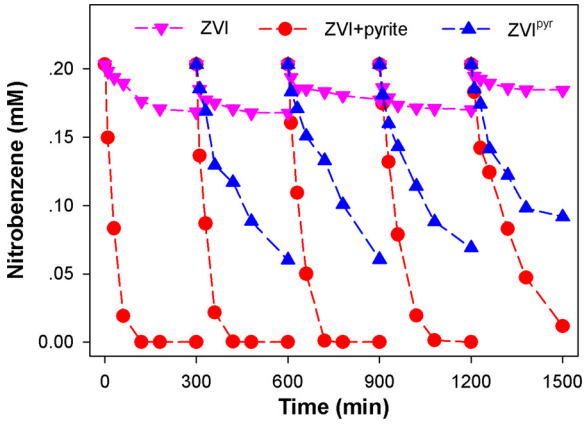

Fig. 4. Nitrobenzene removal by ZVI alone or ZVI/pyrite mixture for five successive runs (0–300, 300–600, 600–900, 900–1200 and 1200–1500 min), and by the recycled ZVI^{pyr} (separated from the solid residue after first-run reaction of nitrobenzene with ZVI/pyrite mixture) for four successive runs (300–600, 600–900, 900–1200 and 1200–1500 min). The pH_0 for each run is 6.0.

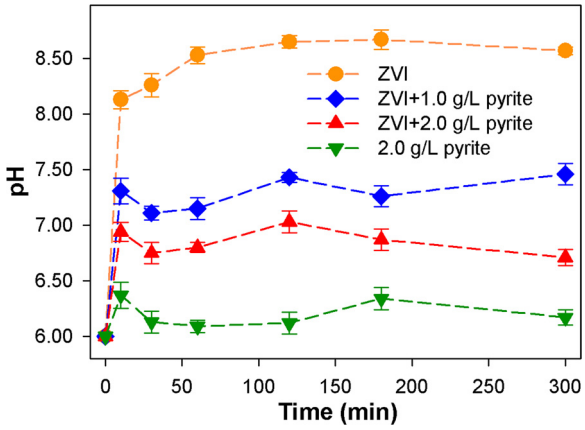

Fig. 5. pH variation during nitrobenzene reduction by ZVI (0.5 g/L), pyrite and their mixtures, pH_0 = 6.0.

3.3. Generation of reactive Fe^{2+} in the combined ZVI/pyrite system

The reactions shown in Eqs. (2) and (5) indicate there should be Fe^{2+} produced in the combined ZVI/pyrite system, and it is well known that Fe^{2+} adsorbed on iron-containing minerals can effectively reduce nitrobenzene and its substituted derivatives [61]. In this heterogeneous system containing solid ZVI and pyrite, however, little free Fe^{2+} was detected in aqueous phase, which is associated with the adsorption of Fe^{2+} onto pyrite or iron (hydr)oxides generated on iron surface and then the quick oxidation of Fe^{2+} by nitrobenzene [45]. A simulation experiment for validating this hypothesis was carried out by dropwise addition of 0.10 mmol/L of Fe^{3+} into systems containing ZVI, pyrite, and the ZVI/pyrite mixture at the buffered pH of 6.0 and 7.0, which is close to the pH observed in the reaction system of nitrobenzene with the ZVI/pyrite mixture (0.5 + 2.0 g/L). The results in Fig. 6(a) revealed that pyrite played a dominant role in reducing Fe^{3+} in the combined ZVI/pyrite system because much more Fe^{2+} was detected in the reaction system of Fe^{3+} with pyrite than that with ZVI at either pH 6.0 or 7.0, and ZVI with pyrite had a synergistic effect on Fe^{3+} reduction by producing more Fe^{2+} than the sum of that produced separately in the systems of ZVI and pyrite alone.

It is well known that 1,10-phenanthroline could form stable complex with Fe(II) and thus deteriorate the reducing ability of Fe(II) [33,62]. According to the results shown in Fig. 6(b), the presence of 1,10-phenanthroline significantly suppressed the transformation of

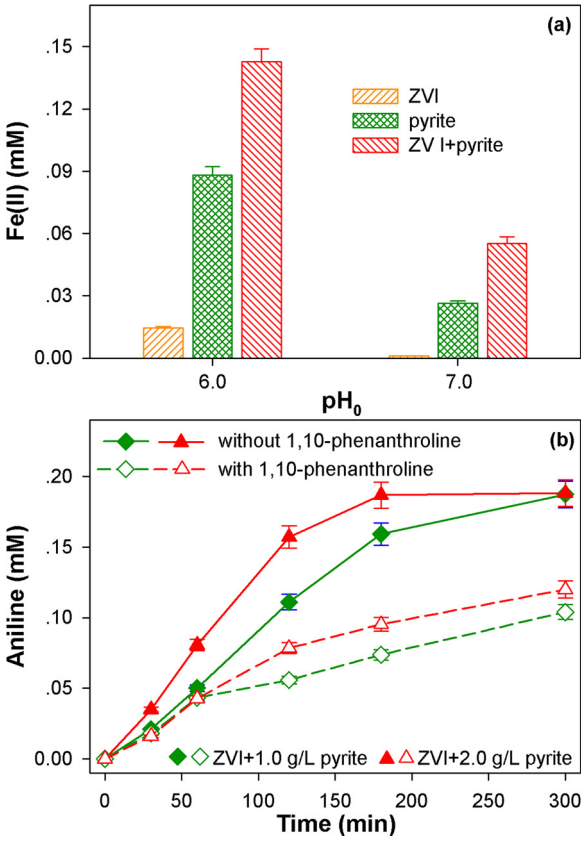

Fig. 6. (a) Production of Fe(II) by dropwise addition of Fe(III) (0.10 mmol/L) into systems containing ZVI, pyrite, and their mixture at buffered pH of 6.0 and 7.0; (b) Influence of 1,10-phenanthroline (6.67 mmol/L) on aniline production during nitrobenzene removal by ZVI/pyrite mixture at pH_0 = 6.0.

nitrobenzene into aniline, confirming the contribution of Fe^{2+} to the reductive removal of nitrobenzene in the ZVI/pyrite system. Therefore, it can be suspected that pyrite can promote the generation of Fe^{2+} in the combined ZVI/pyrite system [55], and the generated Fe^{2+} was quickly adsorbed on the solid surface. The surface-adsorbed Fe^{2+}, especially those bound to iron sulfides were reported to be more reactive than free ions according to previous reports [61,73,64], and could reduce nitrobenzene to aniline according to the reaction (6). The generated Fe^{3+} tended to be reduced by pyrite and/or ZVI to Fe^{2+} again. Thus, the presence of pyrite facilitated the Fe^{3+}/Fe^{2+} cycling, and promoted the reduction of nitrobenzene by ZVI.

$$6Fe^{2+}{}_{(ads)} + Ar-NO_2 + 6H^+ \rightarrow 6Fe^{3+}{}_{(ads)} + Ar-NH_2 + 2H_2O \quad (6)$$

$$+ FeS_2\,(fast)\,/\,Fe^0\,(slow)$$

3.4. Surface activation mechanisms of ZVI by pyrite

The contribution of ZVI surface activation by pyrite to the enhanced decomposition of nitrobenzene was also proposed considering that the reactivity of recycled ZVI in the repetitive experiments was much higher than that of pristine ZVI (Fig. 4). The properties of the recycled ZVI samples were examined with spectroscopic analyses so as to clarify the mechanisms. Fig. 7 shows the XRD patterns of ZVI samples separated from the solid phase after reaction of nitrobenzene with ZVI alone and ZVI/pyrite mixture, respectively. As expected, formation of oxides (Fe_2O_3, hematite) was observed in the solid sample recycled from the system of ZVI alone (Fig. 7(a)). Interestingly, for the two ZVI samples recycled from the ZVI/pyrite mixture, a characteristic peak of hexagonal FeS crystal (troilite, JCPDS No. 01-1247) was observed at 2θ = 43.917° [65], besides the peaks belonging to Fe^0 (2θ = 44.7° and

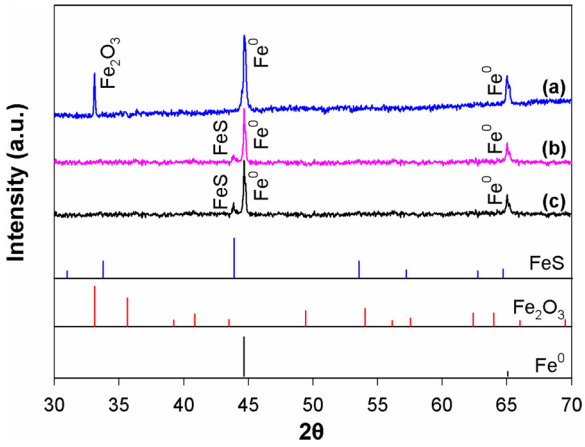

Fig. 7. XRD patterns of iron samples recycled from the solid phase after reaction of nitrobenzene with: (a) ZVI (0.5 g/L) for 300 min, (b) ZVI/pyrite mixture (0.5 + 2.0 g/L) for 180 min, and (c) ZVI/pyrite mixture (0.5 + 2.0 g/L) for 300 min (pH_0 = 6.0), as well as standard XRD patterns of reference samples.

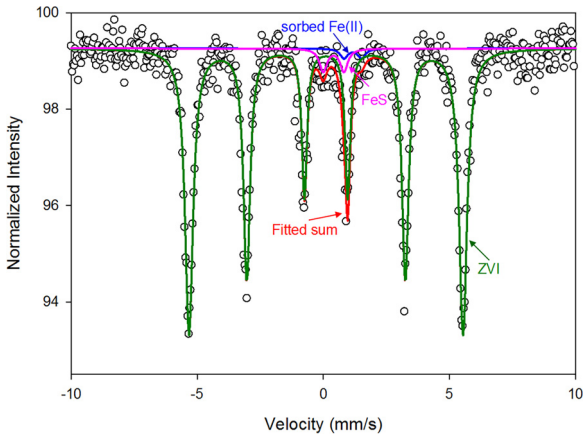

Fig. 8. ^{57}Fe Mössbauer spectrum of the recycled ZVI sample from ZVI/pyrite mixture (0.5 + 2.0 g/L) after reaction for 300 min at pH_0 = 6.0.

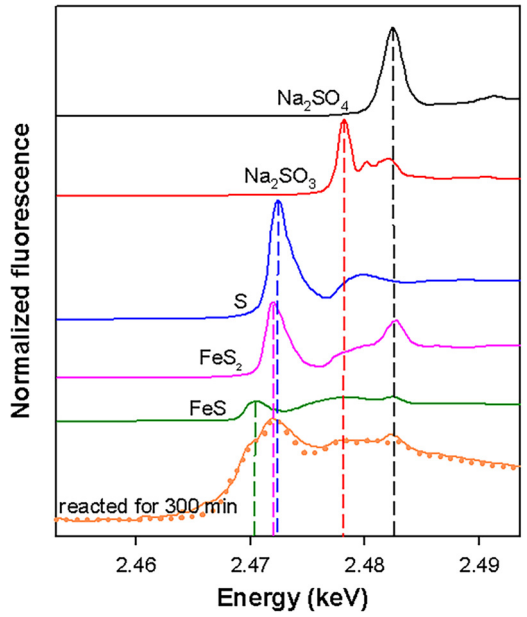

Fig. 9. Sulfur K-edge XANES spectra of five S reference compounds (Na_2SO_4, Na_2SO_3, S, FeS_2 and FeS), and the iron samples recycled from the ZVI/pyrite system (0.5 + 2.0 g/L) after reaction for 300 min at pH_0 = 6.0.

65.0°) (Fig. 7(b and c)), confirming the formation of FeS instead of Fe_2O_3 on ZVI surface. ^{57}Fe Mössbauer spectrum of the recycled ZVI present in Fig. 8 reveals that the solid phase consists of three components, i.e. Fe^0, FeS, and adsorbed Fe^{2+}, which accounted for 94.9%, 3.6%, and 1.5% (by mass) of the total Fe, respectively. The parameters of FeS doublet (I.S. = 0.406 mm/s, and Q.S. = 0.823 mm/s) are consistent with the synthesized FeS reported by Dékány et al [66]. X-ray absorption near-edge structure (XANES) analysis (Fig. 9) of the recycled ZVI sample also proved the formation of FeS. The measured sulfur K-edge energies for SO_4^{2-}, SO_3^{2-}, S°, S_2^{2-} and S^{2-} were 2482.4, 2478.2, 2472.4, 2472.0 and 2470.5 eV, respectively, which are very close to the values reported previously with an average shift of +0.5 eV [67]. For the iron sample recycled from the combined ZVI/pyrite system, the major S phases were a mixture of SO_4^{2-}, S_2^{2-} and S^{2-}, indicating the partial transformation of pyrite (FeS_2) into sulfate and FeS. The results verified that the *in-situ* ZVI sulfidation (namely formation of highly reactive FeS@Fe) could occur during the reaction of nitrobenzene with ZVI/pyrite mixture, which has never been reported in any previous literature. FeS may be generated from the Reaction (9) between Fe^{2+} and HS^-, and HS^- may be produced by the reaction (7) between Fe^0 and SO_4^{2-} or by the Reaction (8) between water and S_2^{2-} on pyrite surface. SO_4^{2-} species was found on the recycled ZVI sample according to the results of XPS analysis shown in Fig. 10. In contrast, the sulfur intermediate species such as HS- would be readily oxidized by Cr(VI) in our previous research about the removal of Cr(VI) by ZVI/pyrite mixture in the column experiments [55], so that the active FeS could not be formed in the system containing Cr(VI) [68–71].

$$4Fe^0 + SO_4^{2-} + 9H^+ \rightarrow 4Fe^{2+} + HS^- + 4H_2O \quad (7)$$

$$4S_2^{2-} + 4H_2O \rightarrow 7HS^- + SO_4^{2-} + H^+ \quad (8)$$

$$Fe^{2+} + HS^- \rightarrow FeS + H^+ \quad (9)$$

Formation of FeS was further validated by analyzing the recycled ZVI samples with XPS spectroscopy. As demonstrated in Fig. 10, the Fe 2p peaks at 710.4 and 723.8 eV correspond to $2p^{3/2}$ and $2p^{1/2}$ binding energies of Fe(II), respectively, and the S 2p peak at 161.7 eV represents the binding energy of S^{2-}, indicating the formation of FeS on ZVI surface at pH_0 6.0 [33,72,73]. Furthermore, a higher pyrite dosage in the ZVI/pyrite system resulted in a higher content of S^{2-} in the recycled ZVI samples (Fig. 10(e)), suggesting the formation of more FeS on the surface of recycled ZVI. The results in SI Fig. S5 indicated that FeS was generated on ZVI surface at all pH_0 levels examined in this study. In addition, FeS formation can also be found on the surface of recycled ZVI after reaction for 1, 3, or 5 runs in the repetitive experiments (Fig. 11), and the gradual decrease in the amount of S^{2-} in the recycled ZVI with the repetitive run (SI Fig. S6) indicated the consumption of FeS@Fe with reaction. This drop in the amount of FeS@Fe resulted in the decreased reactivity of the recycled ZVI, so that declined efficiency of nitrobenzene removal with the proceeding of repetitive experiments was observed in Fig. 4.

FeS is a good electric conductor with a narrow band gap of 0.1 eV [33,74], which facilitated the electron transfer from Fe^0 core to surface-adsorbed oxidants (e.g. Fe^{3+} and nitrobenzene). Many studies have revealed that sulfidation treatment of nZVI and ZVI could enhance the reactivity of nZVI and ZVI toward both organic pollutants and heavy metals [31,75–78]. In this study, sulfidation of ZVI was achieved *in-situ* when nitrobenzene was treated in the combined ZVI/pyrite system under anaerobic conditions, which facilitated the reduction of nitrobenzene by ZVI. Moreover, FeS is more effective in improving the reductive reactivity of surface bound Fe^{2+} than iron oxides [63]. The FeS_x layer on the S-nZVI is more hydrophobic than the (hydr)oxide layer on the surface of ZVI [39,75], and thus has relatively higher capacity for enriching hydrophobic organic contaminants like nitrobenzene ($\log K_{OW}$ = 1.89) [79]. The enrichment of nitrobenzene on solid surface could facilitate the electron transfer from ZVI to

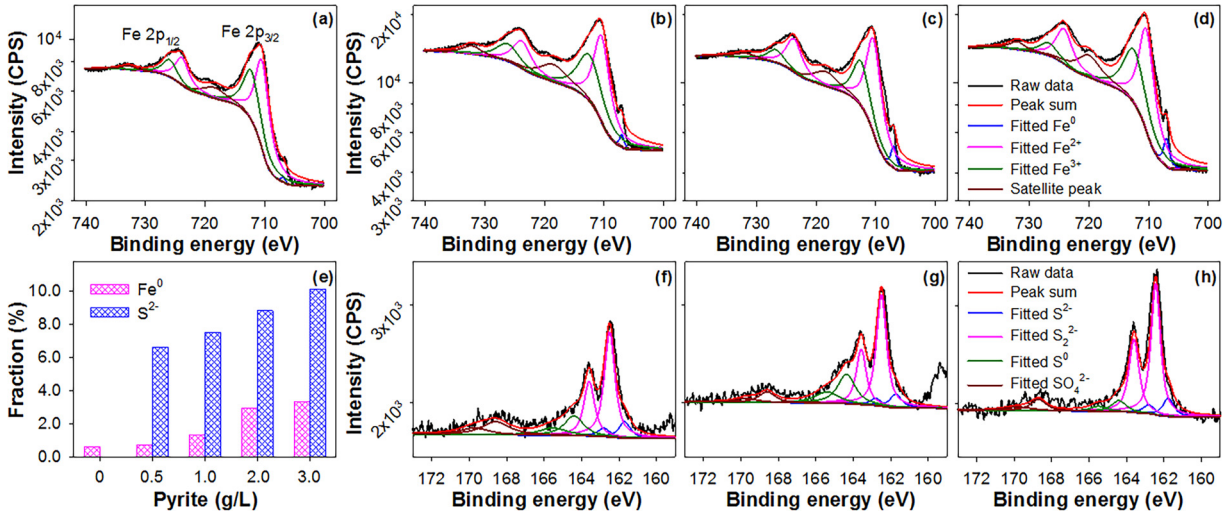

Fig. 10. XPS spectra of Fe 2p (a, b, c, and d) and S 2p (f, g, and h) regions of iron samples recycled from the solid residue after nitrobenzene reduction (for 300 min) by: (a) 0.5 g/L ZVI, (b) and (f) 0.5 g/L ZVI + 1.0 g/L pyrite, (c) and (g) 0.5 g/L ZVI + 2.0 g/L pyrite, (d) and (h) 0.5 g/L ZVI + 3.0 g/L pyrite, pH_0 = 6.0. (e) Fractions (at %) of Fe° and S^{2-} in iron samples recycled from ZVI/pyrite systems of different pyrite dosages.

nitrobenzene, thus accelerating the reduction of nitrobenzene. Accompanying with the formation of FeS, more Fe^0 on the ZVI surface was also observed according to the XPS spectra shown in Fig. 10(b–d), which implies that the formation of passive iron (hydr)oxide at the outmost surface was inhibited. Exposure of Fe^0 makes it readily available for electron transfer to the adsorbed nitrobenzene, so as to facilitate the reaction between ZVI and nitrobenzene.

Furthermore, according to the reactions in Eqs. (2) and (8), SO_4^{2-} was generated in the combined ZVI/pyrite system as a by-product, and peaks belonging to SO_4^{2-} were also observed in XPS spectra of recycled ZVI sample (Figs. 10 and 11, SI Fig. S5). However, little free SO_4^{2-} was detected in the aqueous phase, implying that most of the generated SO_4^{2-} reacted with iron ions (Fe^{2+} or Fe^{3+}) to precipitate as secondary minerals. The formation of solid sulfate salts was validated by acid dissolution of the solid phase recovered from the combined ZVI/pyrite system after reaction with nitrobenzene, as depicted in SI Fig. S7.

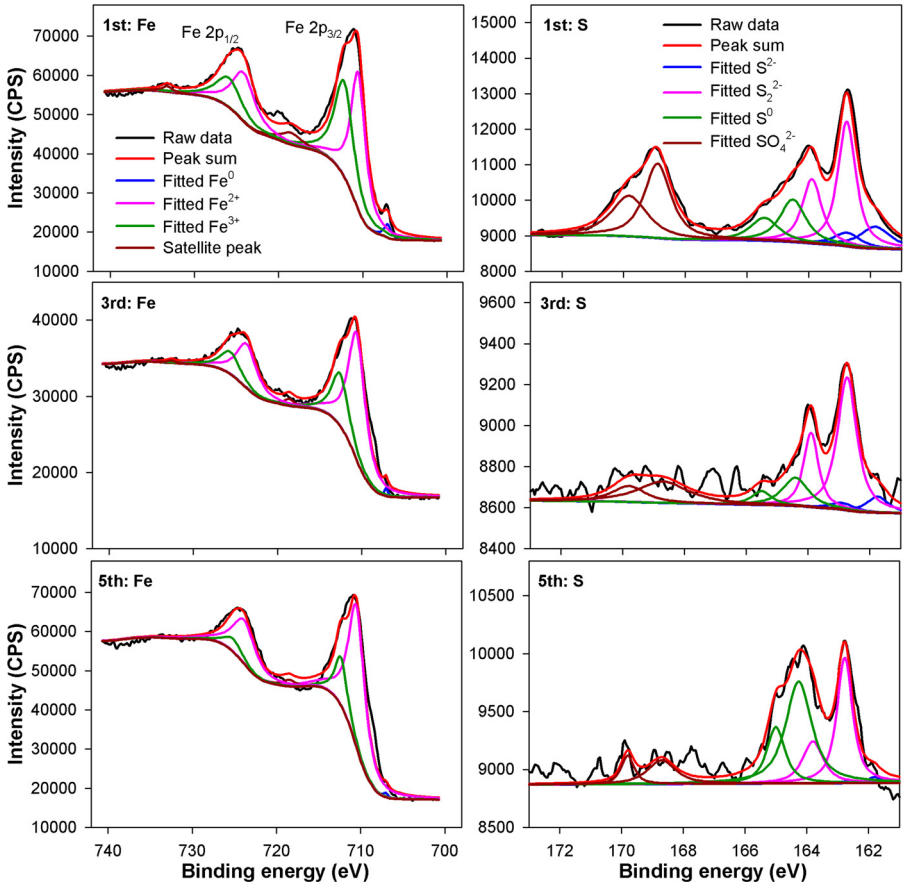

Fig. 11. XPS spectra of Fe 2p (left column) and S 2p (right column) regions of iron samples recycled from the repetitive experiments (after 1 st, 3rd and 5th runs corresponding to reaction time of 0–300, 600–900, and 1200–1500 min, respectively). Reaction conditions: 1.0 g/L ZVI + 4.0 g/L pyrite, pH_0 = 6.0.

Table 1
Surface compositions of some active materials obtained by SEM-EDS analysis.

Sample	Description	Fe(%)	O(%)	S(%)
ZVI	ZVI before reaction	96.6	3.40	0
pyrite	pyrite before reaction	44.7	0	55.3
A	ZVI (0.5 g/L) after reaction	81.8	18.2	0
B	pyrite (2.0 g/L) after reaction	51.0	0	49.0
C[a]	recycled ZVI sample	63.9	34.8	1.24
D[a]	recycled ZVI sample	62.6	35.4	1.98
E[a]	recycled ZVI sample	59.3	37.3	3.52

[a] Sample C) recycled from the ZVI/pyrite system (0.5 + 0.5 g/L), D) recycled from the ZVI/pyrite system (0.5 + 1.0 g/L), and E) recycled from the ZVI/pyrite system (0.5 + 2.0 g/L).

Lipczynska-Kochany et al. [52] reported that sulfate could remove the passive oxide film, while Satapanajaru et al. [80] observed the formation of green rust (GR(II), $[Fe^{II}_4Fe^{III}_2(OH)_{12}][SO_4{\cdot}3H_2O]$) in a reaction system composed of Fe^0 and $FeSO_4$. The positive role of SO_4^{2-} for nitrobenzene removal by ZVI is confirmed by the results shown in SI Fig. S8. Addition of SO_4^{2-} in the solution accelerated the nitrobenzene removal by ZVI, and the higher SO_4^{2-} concentration resulted in quicker removal of nitrobenzene. Thus, it was supposed that the activation of ZVI by pyrite may also be related to the generation of SO_4^{2-} as the by-product of pyrite oxidation, although the specific forms of sulfates need to be determined.

SEM-EDS analysis of the active materials before and after reaction gives more information about their surface compositions. According to the results shown in Table 1 and SI Fig. S9, the increased oxygen content of ZVI after reaction (Sample A) in comparison with ZVI before reaction indicates the formation of iron oxide film that inhibited the reactivity of ZVI alone, while no oxygen observed on the pyrite after reaction (Sample B) implies that pyrite did not participate in the direct reduction of nitrobenzene. The dramatically increased oxygen content (34.8%–37.3%) on the iron sample recycled from the reaction systems of ZVI/pyrite mixtures (Samples C, D and E) indicate that more iron oxide was formed in these systems, which should be resulted from the more consumption of ZVI for reduction of more nitrobenzene. Sulfur on the surface of recycled ZVI samples is consistent with the XPS and Mössbauer results, confirming again the formation of sulfur-containing matter such as FeS and/or sulfates on the ZVI surface. And more sulfur-containing matter was formed with higher dosage of pyrite used in the mixture, according to the change of sulfur content in samples C, D and E. These sulfur-containing matters, especially FeS facilitated electron transfer through the iron oxide film on ZVI surface. In previous reports by Demiya et al. [51] and Shiba et al. [81], the enhanced dechlorination by the mixture of iron and iron sulfides has been explained by the anode (Fe) – cathode (FeS or FeS_2) reaction, which may also contribute to the enhanced nitrobenzene removal in ZVI/pyrite system in this study.

Fig. 12 summarizes the transformation of Fe and S species in the combined ZVI/pyrite system. The proposed mechanisms involve electron transfer from Fe° and adsorbed Fe^{2+} to nitrobenzene, which was reduced into aniline accompanying with the oxidation of Fe^{2+} into Fe^{3+} through the Reaction (6). Then, Fe^{2+} was regenerated through the Reaction (2) of Fe^{3+} with pyrite and Fe^0. The generation of by-products H^+ and SO_4^{2-} from the Reaction (2), and FeS@Fe formed by the pyrite-related Reactions (8) and (9) accelerated further the reduction of nitrobenzene.

4. Conclusions

The presence of pyrite, a ubiquitous mineral in reducing environments, appreciably enhanced the reductive removal of nitrobenzene by ZVI, with the rate constant k_{obs} lifted with increasing pyrite dosage. Moreover, the dosing of pyrite greatly expanded the applicable pH range of ZVI for nitrobenzene removal. The mechanism study indicated that pyrite played multiple roles in accelerating the nitrobenzene removal by ZVI. It could suppress the pH increase in reaction media, facilitate the regeneration of Fe^{2+} and activate the ZVI surface by forming FeS@Fe. This research provides a cost-efficient way for enhancing the performance of ZVI technology by using pyrite that is generally thought to be a kind of mine waste. The mechanism investigation is significant for understanding the long run mechanism of ZVI reactive material in groundwater remediation, because there is a big chance for co-existence of pyrite with ZVI in the remediation site when the wide distribution and easy formation of iron sulfides in anaerobic environment are considered.

Acknowledgements

This work was supported by the National Natural Science Foundation of China (Nos. 21477081, 21777103, 21777117), and Shanghai Science and Technology Committee (17DZ1202203).

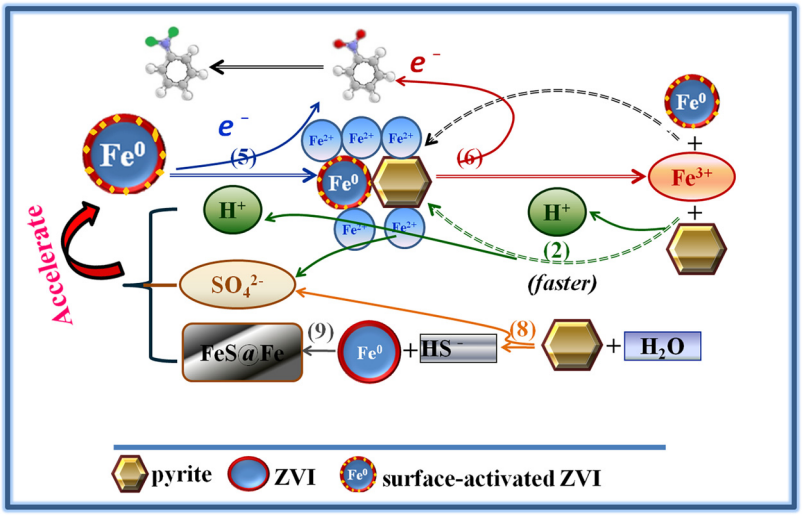

Fig. 12. Schematic transformations of Fe and S species and electron transfer in the reaction system of nitrobenzene with ZVI/pyrite mixture. The numbers in parentheses represent the serial number of formulas listed in the text.

Appendix A. Supplementary data

Supplementary material related to this article can be found, in the online version, at doi:https://doi.org/10.1016/j.apcatb.2018.09.086.

References

[1] R.W. Gillham, S.F. Ohannesin, Enhanced degradation of halogenated aliphatics by zero-valent iron, Ground Water 32 (1994) 958–967.
[2] J.F. Li, Y.M. Li, Q.L. Meng, Removal of nitrate by zero-valent iron and pillared bentonite, J. Hazard. Mater. 174 (2010) 188–193.
[3] Y. Segura, F. Martínez, J.A. Melero, Effective pharmaceutical wastewater degradation by Fenton oxidation with zero-valent iron, Appl. Catal. B-Environ. 136 (2013) 64–69.
[4] F.L. Fu, D.D. Dionysiou, H. Liu, The use of zero-valent iron for groundwater remediation and wastewater treatment: a review, J. Hazard. Mater. 267 (2014) 194–205.
[5] L.P. Liang, W. Sun, X.H. Guan, Y.Y. Huang, W.Y. Choi, H.L. Bao, L.N. Li, Z. Jiang, Weak magnetic field significantly enhances selenite removal kinetics by zero valent iron, Water Res. 49 (2014) 371–380.
[6] Y. Hwang, P.D. Mines, M.H. Jakobsen, H.R. Andersen, Simple colorimetric assay for dehalogenation reactivity of nanoscale zero-valent iron using 4-chlorophenol, Appl. Catal. B-Environ. 166 (2015) 18–24.
[7] J.A. Donadelli, L. Carlos, A. Arques, F.S.G. Einschlag, Kinetic and mechanistic analysis of azo dyes decolorization by ZVI-assisted Fenton systems: pH-dependent shift in the contributions of reductive and oxidative transformation pathways, Appl. Catal. B-Environ. 231 (2018) 51–61.
[8] D.H. Phillips, T. Van Nooten, L. Bastiaens, M.I. Russell, K. Dickson, S. Plant, J.M.E. Ahad, T. Newton, T. Elliot, R.M. Kalin, Ten year performance evaluation of a field-scale zero-valent iron permeable reactive barrier installed to remediate trichloroethene contaminated groundwater, Environ. Sci. Technol. 44 (2010) 3861–3869.
[9] X. Guan, Y. Sun, H. Qin, J. Li, I.M.C. Lo, D. He, H. Dong, The limitations of applying zero-valent iron technology in contaminants sequestration and the corresponding countermeasures: the development in zero-valent iron technology in the last two decades (1994–2014), Water Res. 75 (2015) 224–248.
[10] I.H. Yoon, K.W. Kim, S. Bang, M.G. Kim, Reduction and adsorption mechanisms of selenate by zero-valent iron and related iron corrosion, Appl. Catal. B-Environ. 104 (2011) 185–192.
[11] W.X. Zhang, Nanoscale iron particles for environmental remediation: an overview, J. Nanopart. Res. 5 (2003) 323–332.
[12] S.R. Kanel, B. Manning, L. Charlet, H. Choi, Removal of arsenic(III) from groundwater by nanoscale zero-valent iron, Environ. Sci. Technol. 39 (2005) 1291–1298.
[13] Y.H. Hwang, D.G. Kim, H.S. Shin, Effects of synthesis conditions on the characteristics and reactivity of nano scale zero valent iron, Appl. Catal. B-Environ. 105 (2011) 144–150.
[14] S. Bae, S. Gim, H. Kim, K. Hanna, Effect of $NaBH_4$ on properties of nanoscale zero-valent iron and its catalytic activity for reduction of p-nitrophenol, Appl. Catal. B-Environ. 182 (2016) 541–549.
[15] L. Tan, S. Lu, Z. Fang, W. Cheng, E.P. Tsang, Enhanced reductive debromination and subsequent oxidative ring-opening of decabromodiphenyl ether by integrated catalyst of nZVI supported on magnetic Fe_3O_4 nanoparticles, Appl. Catal. B-Environ. 200 (2017) 200–210.
[16] D. O'Carroll, B. Sleep, M. Krol, H. Boparai, C. Kocur, Nanoscale zero valent iron and bimetallic particles for contaminated site remediation, Adv. Water Resour. 51 (2013) 104–122.
[17] B. Lai, Y. Zhang, Z. Chen, P. Yang, Y. Zhou, J. Wang, Removal of p-nitrophenol (PNP) in aqueous solution by the micron-scale iron–copper (Fe/Cu) bimetallic particles, Appl. Catal. B-Environ. 144 (2014) 816–830.
[18] Y. Gao, F.F. Wang, Y. Wu, R. Naidu, Z.L. Chen, Comparison of degradation mechanisms of microcystin-LR using nanoscale zero-valent iron (nZVI) and bimetallic Fe/Ni and Fe/Pd nanoparticles, Chem. Eng. J. 285 (2016) 459–466.
[19] Y. Sun, X. Guan, J. Wang, X. Meng, C. Xu, G. Zhou, Effect of weak magnetic field on arsenate and arsenite removal from water by zerovalent iron: an XAFS investigation, Environ. Sci. Technol. 48 (2014) 6850–6858.
[20] F. He, D.Y. Zhao, Manipulating the size and dispersibility of zerovalent iron nanoparticles by use of carboxymethyl cellulose stabilizers, Environ. Sci. Technol. 41 (2007) 6216–6221.
[21] Y.B. Hu, X.Y. Li, Influence of a thin aluminum hydroxide coating layer on the suspension stability and reductive reactivity of nanoscale zero-valent iron, Appl. Catal. B-Environ. 226 (2018) 554–564.
[22] Y. Hwang, Y.C. Lee, P.D. Mines, Y.S. Huh, H.R. Andersen, Nanoscale zero-valent iron (nZVI) synthesis in a Mg-aminoclay solution exhibits increased stability and reactivity for reductive decontamination, Appl. Catal. B-Environ. 147 (2014) 748–755.
[23] Y. Li, W. Cheng, G. Sheng, J. Li, H. Dong, Y. Chen, L. Zhu, Synergetic effect of a pillared bentonite support on Se(VI) removal by nanoscale zero valent iron, Appl. Catal. B-Environ. 174 (2015) 329–335.
[24] S.A. Messele, O.S.G.P. Soares, J.J.M. Órfão, F. Stüber, C. Bengoa, A. Fortuny, A. Fabregat, J. Font, Zero-valent iron supported on nitrogen-containing activated carbon for catalytic wet peroxide oxidation of phenol, Appl. Catal. B-Environ. 154 (2014) 329–338.
[25] W. Teng, J.W. Fan, W. Wang, N. Bai, R. Liu, Y. Liu, Y.H. Deng, B. Kong, J.P. Yang, D.Y. Zhao, W.X. Zhang, Nanoscale zero-valent iron in mesoporous carbon (nZVI@C): stable nanoparticles for metal extraction and catalysis, J. Mater. Chem. 5 (2017) 4478–4485.
[26] S. Giri, M. Bhaumik, R. Das, V.K. Gupta, A. Maity, Dehalogenation of aromatic halides by polyaniline/zero-valent iron composite nanofiber: kinetics and mechanisms, Appl. Catal. B-Environ. 202 (2017) 207–216.
[27] D.Y. Shi, X. Zhang, J.J. Wang, J. Fan, Highly reactive and stable nanoscale zero-valent iron prepared within vesicles and its high-performance removal of water pollutants, Appl. Catal. B-Environ. 221 (2018) 610–617.
[28] E.J. Kim, J.H. Kim, A.M. Azad, Y.S. Chang, Facile synthesis and characterization of Fe/FeS nanoparticles for environmental applications, ACS Appl. Mater. Interfaces 3 (2011) 1457–1462.
[29] D.M. Fan, Y. Lan, P.G. Tratnyek, R.L. Johnson, J. Filip, D.M. O'Carroll, A.N. Garcia, A. Agrawal, Sulfidation of iron-based materials: a review of processes and implications for water treatment and remediation, Environ. Sci. Technol. 51 (2017) 13070–13085.
[30] J. Li, X. Zhang, Y. Sun, L. Liang, B. Pan, W. Zhang, X. Guan, Advances in sulfidation of zerovalent iron for water decontamination, Environ. Sci. Technol. 51 (2017) 13533–13544.
[31] Y. Gu, B. Wang, F. He, M.J. Bradley, P.G. Tratnyek, Mechanochemically sulfidated microscale zero valent iron: Pathways, kinetics, mechanism, and efficiency of trichloroethylene dechlorination, Environ. Sci. Technol. 51 (2017) 12653–12662.
[32] D. Fan, G.O.B. Johnson, P.G. Tratnyek, R.L. Johnson, Sulfidation of nano zerovalent iron (nZVI) for improved selectivity during in-situ chemical reduction (ISCR), Environ. Sci. Technol. 50 (2016) 9558–9565.
[33] J. Du, J. Bao, C. Lu, D. Werner, Reductive sequestration of chromate by hierarchical FeS@Fe° particles, Water Res. 102 (2016) 73–81.
[34] S. Song, Y. Su, A.S. Adeleye, Y. Zhang, X. Zhou, Optimal design and characterization of sulfide-modified nanoscale zerovalent iron for diclofenac removal, Appl. Catal. B-Environ. 201 (2017) 11–220.
[35] Q. Shao, C. Xu, Y. Wang, S. Huang, B. Zhang, L. Huang, D. Fan, P.G. Tratnyek, Dynamic interactions between sulfidated zerovalent iron and dissolved oxygen: mechanistic insights for enhanced chromate removal, Water Res. 135 (2018) 322–330.
[36] J. Li, X. Zhang, M. Liu, B. Pan, W. Zhang, Z. Shi, X. Guan, Enhanced reactivity and electron selectivity of sulfidated zerovalent iron toward chromate under aerobic conditions, Environ. Sci. Technol. 52 (2018) 2988–2997.
[37] H. Zou, E. Hu, S. Yang, L. Gong, F. He, Chromium (VI) removal by mechanochemically sulfidated zero valent iron and its effect on dechlorination of trichloroethene as a co-contaminant, Sci. Total Environ. 650 (2019) 419–426.
[38] M.L. Coleman, D.B. Hedrick, D.R. Lovley, D.C. White, K. Pye, Reduction of Fe(III) in sediments by sulfate-reducing bacteria, Nature 361 (1993) 436–438.
[39] R. Weerasooriya, B. Dharmasena, Pyrite-assisted degradation of trichloroethene (TCE), Chemosphere 42 (2001) 389–396.
[40] W. Lee, B. Batchelor, Abiotic reductive dechlorination of chlorinated ethylenes by iron-bearing soil minerals. 1. Pyrite and magnetite, Environ. Sci. Technol. 36 (2002) 5147–5154.
[41] C. Kantar, M.S. Bulbul, Effect of pH-buffering on Cr(VI) reduction with pyrite in the presence of various organic acids: continuous-flow experiments, Chem. Eng. J. 287 (2016) 173–180.
[42] L. Charlet, M.L. Kang, F. Bardelli, R. Kirsch, A. Gehin, J.M. Greneche, F.R. Chen, Nanocomposite pyrite-greigite reactivity toward Se(IV)/Se(VI), Environ. Sci. Technol. 46 (2012) 4869–4876.
[43] S. Bae, D. Kim, W. Lee, Degradation of diclofenac by pyrite catalyzed Fenton oxidation, Appl. Catal. B-Environ. 134 (2013) 93–102.
[44] Y.Y. Gong, J.C. Tang, D.Y. Zhao, Application of iron sulfide particles for groundwater and soil remediation: a review, Water Res. 89 (2016) 309–320.
[45] C.O. Moses, J.S. Herman, Pyrite oxidation at circumneutral pH, Geochim. Cosmochim. Acta 55 (1991) 471–482.
[46] M.L. Kang, F.R. Chen, S.J. Wu, Y.Q. Yang, C. Bruggeman, L. Charlet, Effect of pH on Aqueous Se(IV) reduction by pyrite, Environ. Sci. Technol. 45 (2011) 2704–2710.
[47] T.L. Johnson, M.M. Scherer, P.G. Tratnyek, Kinetics of halogenated organic compound degradation by iron metal, Environ. Sci. Technol. 30 (1996) 2634–2640.
[48] Y.L. Zhang, K. Zhang, C.M. Dai, X.F. Zhou, Performance and mechanism of pyrite for nitrobenzene removal in aqueous solution, Chem. Eng. Sci. 111 (2014) 135–141.
[49] N. Balci, W.C. Shanks, B. Mayer, K.W. Mandernack, Oxygen and sulfur isotope systematics of sulfate produced by bacterial and abiotic oxidation of pyrite, Geochim. Cosmochim. Acta 71 (2007) 3796–3811.
[50] P. Le Pape, M. Blanchard, J. Brest, J.C. Boulliard, M. Ikogou, L. Stetten, S. Wang, G. Landrot, G. Morin, Arsenic incorporation in pyrite at ambient temperature at both tetrahedral S^{-I} and octahedral Fe^{II} sites: evidence from EXAFS-DFT analysis, Environ. Sci. Technol. 51 (2017) 150–158.
[51] M. Demiya, M.A. Uddin, Y. Kato, Enhancement in trichloroethylene dechlorination by mixed particles of iron–iron disulfide or iron–iron sulfide, J. Environ. Chem. Eng. 6 (2018) 1020–1026.
[52] E. Lipczynskakochany, S. Harms, R. Milburn, G. Sprah, N. Nadarajah, Degradation of carbon-tetrachloride in the presence of iron and sulfur-containing-compounds, Chemosphere 29 (1994) 1477–1489.
[53] W.Z. Yin, J.H. Wu, P. Li, X.D. Wang, N.W. Zhu, P.X. Wu, B. Yang, Experimental study of zero-valent iron induced nitrobenzene reduction in groundwater: the effects of pH, iron dosage, oxygen and common dissolved anions, Chem. Eng. J. 184 (2012) 198–204.
[54] Y. Hwang, A. Salatas, P.D. Mines, M.H. Jakobsen, H.R. Andersen, Graduated characterization method using a multi-well microplate for reducing reactivity of nanoscale zero valent iron materials, Appl. Catal. B-Environ. 181 (2016) 314–320.
[55] Y. Lü, Z. Li, J. Li, K. Chen, H. Dong, J. Shou, Y. Li, Synergetic effect of pyrite on Cr (VI) removal by zero valent iron in column experiments: an investigation of

mechanisms, Chem. Eng. J. 349 (2018) 522–529.
[56] H.C. Liu, J.L. Xia, Z.Y. Nie, A.A. Peng, C.Y. Ma, L. Zheng, Y.D. Zhao, Comparative study of sulfur utilization and speciation transformation of two elemental sulfur species by thermoacidophilic *Archaea Acidianus* manzaensis YN-25, Process Biochem. 48 (2013) 1855–1860.
[57] A. Agrawal, P.G. Tratnyek, Reduction of nitro aromatic compounds by zero-valent iron metal, Environ. Sci. Technol. 30 (1996) 153–160.
[58] Y. Mu, H.Q. Yu, J.C. Zheng, S.J. Zhang, G.P. Sheng, Reductive degradation of nitrobenzene in aqueous solution by zero-valent iron, Chemosphere 54 (2004) 789–794.
[59] J. Dong, Y. Zhao, R. Zhao, R. Zhou, Effects of pH and particle size on kinetics of nitrobenzene reduction by zero-valent iron, J. Environ. Sci. China (China) 22 (2010) 1741–1747.
[60] Y.T. Lin, C.P. Huang, Reduction of chromium(VI) by pyrite in dilute aqueous solutions, Sep. Purif. Technol. 63 (2008) 191–199.
[61] J. Klausen, S.P. Troeber, S.B. Haderlein, R.P. Schwarzenbach, Reduction of substituted nitrobenzenes by Fe(II) in aqueous mineral suspensions, Environ. Sci. Technol. 29 (1995) 2396–2404.
[62] L.P. Liang, W.J. Yang, X.H. Guan, J. Li, Z.J. Xu, J. Wu, Y.Y. Huang, X.G.Z. Zhang, Kinetics and mechanisms of pH-dependent selenite removal by zero valent iron, Water Res. 47 (2013) 5846–5855.
[63] K. Pecher, S.B. Haderlein, R.P. Schwarzenbach, Reduction of polyhalogenated methanes by surface-bound Fe(II) in aqueous suspensions of iron oxides, Environ. Sci. Technol. 36 (2002) 1734–1741.
[64] M. Elsner, R.P. Schwarzenbach, S.B. Haderlein, Reactivity of Fe(II)-bearing minerals toward reductive transformation of organic contaminants, Environ. Sci. Technol. 38 (2004) 799–807.
[65] N.M. Pedoussaut, C. Lind, Facile synthesis of troilite, Inorg. Chem. 47 (2008) 392–394.
[66] I. Dékány, L. Turi, Z. Homonnay, A. Vértes, K. Burger, Preparation of nanosize FeS particles on SiO_2 and clay mineral supports: SAXS and Mössbauer spectroscopic measurements, Colloids Surf. A Physicochem. Eng. Asp. 119 (1996) 195–203.
[67] M.E. Fleet, XANES spectroscopy of sulfur in earth materials, J. Bone Miner. Res. 43 (2005) 1811–1838.
[68] K.U. Mayer, D.W. Blowes, E.O. Frind, Reactive transport modeling of an in situ reactive barrier for the treatment of hexavalent chromium and trichloroethylene in groundwater, Water Resour. Res. 37 (2001) 3091–3103.
[69] D. Rickard, G.W. Luther, Chemistry of iron sulfides, Chem. Rev. 107 (2007) 514–562.
[70] E.C. Butler, K.F. Hayes, Factors influencing rates and products in the transformation of trichloroethylene by iron sulfide and iron metal, Environ. Sci. Technol. 35 (2001) 3884–3891.
[71] Y. Lan, E.C. Butler, Iron-sulfide-associated products formed during reductive dechlorination of carbon tetrachloride, Environ. Sci. Technol. 50 (2016) 5489–5497.
[72] F. Demoisson, M. Mullet, B. Humbert, Investigation of pyrite oxidation by hexavalent chromium: solution species and surface chemistry, J. Colloid Interface Sci. 316 (2007) 531–540.
[73] C.H. Xu, B.L. Zhang, Y.H. Wang, Q.Q. Shao, W.Z. Zhou, D.M. Fan, J.Z. Bandstra, Z.Q. Shi, P.G. Tratnyek, Effects of sulfidation, magnetization, and oxygenation on azo dye reduction by zerovalent iron, Environ. Sci. Technol. 50 (2016) 11879–11887.
[74] Y. Xu, M.A.A. Schoonen, The absolute energy positions of conduction and valence bands of selected semiconducting minerals, Am. Mineral. 85 (2000) 543–556.
[75] S.R.C. Rajajayavel, S. Ghoshal, Enhanced reductive dechlorination of trichloroethylene by sulfidated nanoscale zerovalent iron, Water Res. 78 (2015) 144–153.
[76] D. Li, Z. Mao, Y. Zhong, W. Huang, Y. Wu, P. Peng, Reductive transformation of tetrabromobisphenol A by sulfidated nano zerovalent iron, Water Res. 103 (2016) 1–9.
[77] E.J. Kim, J.H. Kim, Y.S. Chang, D. Turcio-Ortega, P.G. Tratnyek, Effects of metal ions on the reactivity and corrosion electrochemistry of Fe/FeS nanoparticles, Environ. Sci. Technol. 48 (2014) 4002–4011.
[78] S. Huang, C. Xu, Q. Shao, Y. Wang, B. Zhang, B. Gao, W. Zhou, P.G. Tratnyek, Sulfide-modified zerovalent iron for enhanced antimonite sequestration: characterization, performance, and reaction mechanisms, Chem. Eng. J. 338 (2018) 539–547.
[79] J. Riedl, R. Altenburger, Physicochemical substance properties as indicators for unreliable exposure in microplate-based bioassays, Chemosphere 67 (2007) 2210–2220.
[80] T. Satapanajaru, P.J. Shea, S.D. Comfort, Y. Roh, Green rust and iron oxide formation influences metolachlor dechlorination during zerovalent iron treatment, Environ. Sci. Technol. 37 (2003) 5219–5227.
[81] M. Shiba, M.A. Uddin, Y. Kato, T. Ono, Degradation of chlorinated organic compounds by mixed particles of iron/iron sulfide or iron/iron disulfide, Mater. Trans. 55 (2014) 708–712.